Influence of disjoining pressure on the dynamics of steadily moving long bubbles inside narrow cylindrical capillaries

Kaustav Chaudhury,[1] Palash V. Acharya,[2] and Suman Chakraborty[1,*]
[1]*Department of Mechanical Engineering, Indian Institute of Technology Kharagpur, Kharagpur–721302, India*
[2]*Department of Mechanical Engineering, National Institute of Technology, Karnataka, Surathkal, India*
(Received 12 August 2013; revised manuscript received 20 March 2014; published 6 May 2014)

We study the influence of disjoining pressure for moving long bubbles inside cylindrical capillaries. Towards that end, consistent thin-film equations, for the annular region separating the bubble from the channel surface, are presented with specific emphasis on three different attributes: (a) the van der Waals interaction, formalized by the classical Lifshitz form of disjoining pressure; (b) the nonuniformity in film thickness, accommodated by the necessary corrections in the disjoining pressure; and (c) the electrostatic component of disjoining pressure, reminiscent of the electrostatic interactions in the presence of surface charges. The present thin-film analysis appositely uncovers the existence and the breakdown of the two-thirds power law for minimum film thickness behavior. This is attributed to the alteration in the characteristic length scales governing the underlying physics, as quantitatively established by our consistent scaling analysis. In the breakdown regimes, the characteristic length scales are found to be composed of the suitable combinations of the capillary number and the physics driven intrinsic length scales. The characteristics of the breakdown regime reported by us appear to match excellently with reported experimental data in the low capillary number regime. Towards unveiling the possible implications of slope and curvature dependence of disjoining pressure, our analysis reveals that the consequent correction term endorses an order two-thirds power of the capillary number contribution without alerting the governing length scales. The subsequent asymptotic analysis reveals that this correction may be neglected to the leading order approximation. Finally, we consider the electrostatic component of the disjoining pressure which may be realized in the presence of surface charges. Our analysis reveals that the significance of the electrostatic interaction is realized over a very small capillary number regime, leading towards the departure from the two-thirds power law type behavior. Reasonably good agreement is obtained with reported experimental data over this regime.

DOI: 10.1103/PhysRevE.89.053002 PACS number(s): 47.61.−k

I. INTRODUCTION

The dynamics of long gaseous bubbles in cylindrical capillaries has been a problem of immense interest to the research community, primarily attributable to a plethora of relevant practical applications and the rich underlying physics involved [1–17]. While the broad characteristic features describing the underlying phenomena have been successfully uncovered by many researchers on employing the traditional thin-film based approach [1,3,6,8,9,11,13,16], several of the consequent inferences have turned out to be questionable in case the length scales under purview demand an additional accounting of small-scale interfacial interactions that may best be represented in terms of the so-called disjoining pressure [17–24] from a pseudo continuum perspective. In fact, in several experimental studies [2,13,25], researchers have attributed plausible deviations from theoretical predictions to a possible nontrivial interplay of the disjoining pressure related effects. However, more studies need to be made on thin-film analysis of the dynamical evolution of bubbles in narrow confined geometries, with a comprehensive accounting of the various facets of disjoining pressure that may become important when the interfacial length scales approach molecular dimensions.

Here we aim to capture the various consequences of disjoining pressure on the dynamical evolution of long gaseous bubbles in cylindrical capillaries, by following the thin-film approach. In the disjoining pressure formalism, we specifically emphasize three distinctive interfacial attributes: (a) the van der Waals interaction, formalized by the classical Lifshitz form of disjoining pressure [17,21,22,26]; (b) the nonuniformity in film thickness, accommodated by the necessary corrections in the disjoining pressure [19,24]; and (c) the electrostatic component of disjoining pressure, reminiscent of the electrostatic interactions, in the presence of surface charges [20,23,27]. Our analysis aptly uncovers, in perfect agreement with previous reported observations, the existence and the breakdown of the celebrated two-thirds power law based estimation [2]. Our results, in effect, reveal that unlike the classical Bretherton scaling [1], the scaling laws derived by taking disjoining pressure into account match excellently with the experimental data in the low capillary number regime, and asymptotically match with the Bretherton scaling as the capillary number is progressively increased. Following this, we bring out the existence of different characteristic length scales under different physical situations. With consistent accounting of those length scales, we unveil the proper functional dependency of the film or bubble profile on the inherent governing parameters, leading towards uncovering the underlying physics, in satisfactory agreement with other reported theoretical and experimental evidences [28–30]. Further, our results demonstrate that while the slope and curvature dependence of disjoining pressure is unlikely to alter the essential physics of interest, incorporation of the electrostatic component of the disjoining pressure may indeed turn out to be important in dictating the interfacial profile. By accounting for the later effects, we effectively

*Corresponding author: suman@mech.iitkgp.ernet.in

delineate that the dynamics of bubbles in the presence of surface charge is primarily dictated by the traction generated on the bubble interface, in the two-thirds power law regime. However, in the very low capillary number regime, the electrostatic component seems to indeed play a significant role, yielding reasonably good agreement between our theoretical predictions and reported experimental data.

II. THE THIN-FILM MODEL

We consider a long gaseous bubble moving with a speed of U inside a cylindrical capillary of radius R, within another immiscible liquid medium of dynamic viscosity μ, as shown in Fig. 1. Over the axial extent, the bubble assumes a cylindrical shape. We focus our attention on the low capillary number regime $\mathrm{Ca} = \mu U/\sigma$ (here σ is the coefficient of surface tension) limit. Under this condition, the bubble shape can be approximated by a hemispherical frontal cap connected to the cylindrical zone through a transition zone, earmarked as a region of rapid curvature change [1–3,6,8,9,11,13,14]. In a perfect wetting scenario, there exists a thin-film region of the background liquid in between the bubble interface and the channel surface [1–3,6,8,9,11,13,14], as highlighted in the magnified portion of Fig. 1.

The basic transport equation over the thin-film region can be given as

$$\left.\begin{aligned} &\text{Momentum:} \quad \frac{\partial p}{\partial x} = \mu \frac{\partial^2 u}{\partial y^2} \\ &\text{Continuity:} \quad \frac{\partial}{\partial x}\int_0^{h(x)} u\,dy = 0 \end{aligned}\right\}, \tag{1}$$

where u and p represent the velocity along the x direction, and pressure, respectively. To supplement Eq. (1), the no-slip boundary condition at the channel surface is considered throughout. To incorporate the surface charge effect, it is usual to add some surfactant that allows the accumulation of charges over the bubble surface, in addition to the charge accumulation over the channel surface [13]. Over the surfactant-laden bubble interface, we consider the no-slip boundary condition [13],

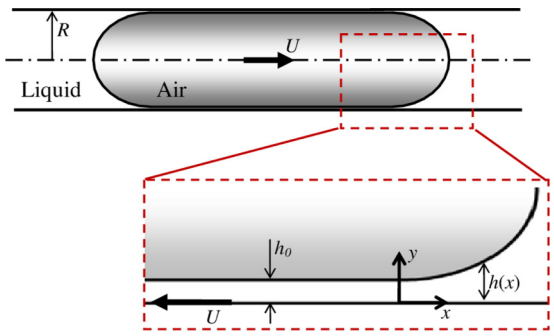

FIG. 1. (Color online) Schematic of a long gaseous bubble moving with speed U inside a cylindrical capillary of radius R, within another immiscible liquid medium. In the magnified portion, we show the thin-film region. The reference frame x-y moves with the bubble. Thus, with respect to the x-y frame, the bubble appears motionless, but the channel moves with speed U in the opposite direction, as indicated in the magnified portion. Here $h(x)$ represents the thin-film profile and h_0 represents the minimum film thickness.

and zero shear stress condition otherwise. The contribution of pressure can be obtained from normal stress balance over the interfacial region as

$$p = p_0 - \sigma \frac{\partial^2 h}{\partial x^2} + \Sigma, \tag{2}$$

where p_0 denotes the pressure from the gas side and $\sigma\,\partial^2 h/\partial x^2$ denotes the Young-Laplace pressure jump across the interface. The term Σ in Eq. (2) denotes the pressure contribution due to additional interfacial interactions and energetics. Using physics driven specific forms of Σ, we solve Eqs. (1) and (2) to obtain the situation specific thin-film equations which serve as the models for the subsequent analyses.

III. INFLUENCE OF THE VAN DER WAALS INTERACTION

The van der Waals interaction has its molecular origin. However, its implications from a continuum perspective may be brought out from the fundamental principle of free energy minimization over the interfacial region. This results in disjoining pressure (Π) contribution in the normal stress balance as [17,21,22,26]

$$p = p_0 - \sigma \frac{\partial^2 h}{\partial x^2} \underbrace{- \frac{A_H}{6\pi h^3}}_{\Sigma = \Pi}, \tag{3}$$

where A_H is the Hamaker constant. This form of Π is often elucidated as the Lifshitz form of disjoining pressure [17,21,22,26]. With this argument, along with Eq. (1), one can obtain the thin-film equation of the form

$$\frac{\partial}{\partial x}\left(h^3 \frac{\partial^3 h}{\partial x^3}\right) = 3\mathrm{Ca}\frac{\partial h}{\partial x} + R_m^2 \frac{\partial}{\partial x}\left(\frac{1}{h}\frac{\partial h}{\partial x}\right), \tag{4}$$

with $R_m = \sqrt{|A_H|/2\pi\sigma}$, popularly known as the molecular length scale [28,29]. From Eq. (4) we can say that taking disjoining pressure into account, the thin-film profile can be given in a functional form as $h \equiv h\,(x; R_m, \mathrm{Ca})$, depending on both intrinsic molecular length scale (R_m), representing the physics driven intrinsic length scale for the physical paradigm under consideration, and the capillary number Ca.

First, we solve Eq. (4) with the initial condition

$$\lim_{x\to-\infty} h \to h_0, \quad \text{and} \quad \lim_{x\to-\infty} \frac{\partial^n h}{\partial x^n} \to 0, \quad \text{for } n \geqslant 1 \text{ being a real integer.} \tag{5}$$

The solution is iteratively matched with the condition

$$\lim_{x\to\infty} \frac{\partial^2 h}{\partial x^2} \to \frac{1}{R}. \tag{6}$$

The variation of h_0/R, so obtained, is plotted against Ca in Fig. 2. For the sake of comprehensiveness, we present Chen's experimental observations, with soltrol-220 and air bubbles [2]. In the same figure, we also indicate the two-thirds power law based estimation [1] $h_0/R = 0.643(3\mathrm{Ca})^{2/3}$. The dotted line in the figure represents the solution of rescaled Eq. (16); details regarding its implication are delineated *a posteriori*. First of all, from Fig. 2, one can make a very important inference: The minimum film thickness behavior

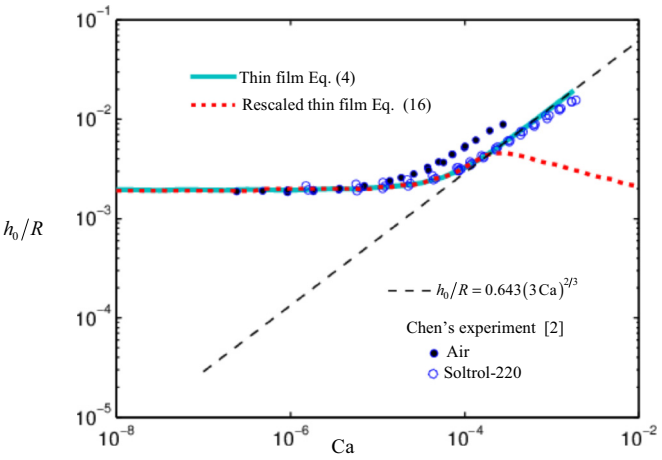

FIG. 2. (Color online) Variation of h_0/R with Ca.

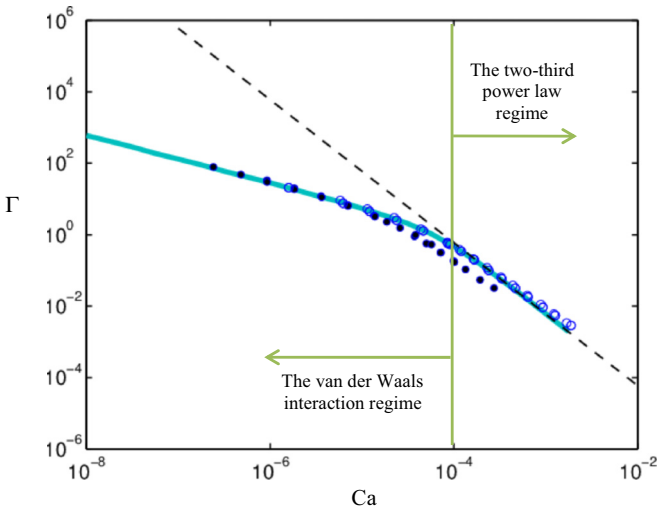

FIG. 3. (Color online) Variation of Γ with Ca. The markers and the line styles have the same meaning as in the Fig. 2. The two-thirds power law and the van der Waals interaction regimes are also highlighted in the figure. However, the demarcation between these two regimes is not as sharp as shown here; the present demarcation is to be considered as the representative demonstration of the essential feature.

obeys the two-thirds power law in a somewhat higher capillary number regime ($\mathrm{Ca} > 10^{-4}$) whereas a marked departure from that, in the very low capillary number regime ($\mathrm{Ca} \ll 10^{-4}$), is evident. From the perfect agreement between the reported experimental observation and the present thin-film model, the enticing influence of the van der Waals interaction is apparent. Thus, we denote this breakdown regime as the van der Waals interaction regime. It is now, therefore, imperative to unveil the underlying physics leading to such behavior, as we endeavor in the subsequent sections.

A. The two-thirds power law regime

The two-thirds power law regime, following Bretherton scaling analysis [1], is governed by the length scales h_0 and $h_0/(3\mathrm{Ca})^{1/3}$ for the variables h and x in Eq. (4). Using these scales we obtain the normalized thin-film equation as

$$\underbrace{\frac{\partial}{\partial\eta}\left(F^3\frac{\partial^3 F}{\partial\eta^3}\right)}_{\Lambda_1} = \underbrace{\frac{\partial F}{\partial\eta}}_{\Lambda_2} + \Gamma\underbrace{\frac{\partial}{\partial\eta}\left(\frac{1}{F}\frac{\partial F}{\partial\eta}\right)}_{\Lambda_3}, \tag{7}$$

where $\eta = x\,(3\mathrm{Ca})^{1/3}/h_0$, $F\,(\eta;\Gamma) = h/h_0$. The factor $\Gamma = R_m^2/h_0^2\,(3\mathrm{Ca})^{2/3}$ defines the order of magnitude of the disjoining pressure contribution due to van der Waals interaction $\Gamma = O\,(\Lambda_3)$. Considering $A_H \approx 10^{-20}$ J and $\sigma = 0.072$ J/m^2 (for air bubble in water) [17,29], we estimate the possible values of Γ. For the sake of comprehensiveness, in Fig. 3, we plot the variation of Γ with Ca, as obtained from the solution of Eq. (4), Chen's [2] experimental data, and as predicted by the two-thirds power law. From the figure, it is noteworthy that $\Gamma \ll 1$ in the two-thirds power law regime. It is also evident that Γ approaches $O\,(1)$ as the breakdown is approached, and finally assumes a very high value in the van der Waals interaction regime.

Therefore, in this two-thirds power law regime, we can expand the film profile function $F\,(\eta;\Gamma)$ as

$$F(\eta;\Gamma) = F_0(\eta) + \Gamma F_1(\eta) + O(\Gamma^2). \tag{8}$$

With this argument the thin-film equation Eq. (7) reduces to the forms, at different orders, as

$$\begin{aligned} O(\Gamma^0):&\ \frac{\partial}{\partial\eta}\left(F_0^3\frac{\partial^3 F_0}{\partial\eta^3}\right) = \frac{\partial F_0}{\partial\eta},\\ O(\Gamma^1):&\ \frac{\partial}{\partial\eta}\left(F_0^3\frac{\partial^3 F_1}{\partial\eta^3} + 3F_0^2F_1\frac{\partial^3 F_0}{\partial\eta^3}\right)\\ &= \frac{\partial F_1}{\partial\eta} + \frac{\partial}{\partial\eta}\left(\frac{1}{F_0}\frac{\partial F_0}{\partial\eta}\right). \end{aligned} \tag{9}$$

Evidently, the leading order approximation represents the classical Bretherton-Landau-Levich formalism. Following this Eq. (9) and the corresponding scaling, one can obtain, to the leading order approximation,

$$\frac{h_0}{R} = \left(\lim_{\eta\to\infty}\frac{\partial^2 F_0}{\partial\eta^2}\right)(3\mathrm{Ca})^{2/3}. \tag{10}$$

Upon solving Eq. (9), one can further obtain $\lim_{\eta\to\infty}\partial^2 F_0/\partial\eta^2 = 0.643$, which recovers the celebrated two-thirds power law [1]. Thus we have seen that the validity of Bretherton scaling estimations [1] and subsequent two-thirds power law based estimation of minimum film thickness behavior is decided by the order of magnitude of $\Gamma = R_m^2/h_0^2(3\mathrm{Ca})^{2/3}$, essentially defining the contribution of disjoining pressure. However, as Γ approaches $O\,(1)$ or higher values, the thin-film equation (7) cannot be reduced to the Bretherton-Landau-Levich formalism. Moreover, in the very low capillary number regime ($\mathrm{Ca} \ll 10^{-4}$), we have $\Gamma \gg 1$. Thus, Eq. (7) essentially gets reduced to $R_m^2\partial(h^{-1}\partial h/\partial x)/\partial x \approx 0$, in dimensional form. This consideration is nevertheless unphysical, since it shows that the disjoining pressure effect is not even balanced by surface tension. This is suggestive of a very important aspect: The underlying physics may be governed by characteristic

length scales that are somewhat different from the traditional physical scales considered *a priori*.

B. The van der Waals interaction regime

Our anticipation regarding the alteration in bubble dynamics due to the alteration in the characteristic length scales requires consistent scaling analysis and subsequent unfolding of the observed behaviors. For consistent scaling analysis, first we begin with the stretching transformation of the form

$$x = \ell_x \eta \quad \text{and} \quad h = \ell_h F, \tag{11}$$

with η and F as the transformed variables where ℓ_x and ℓ_h are the corresponding scales for stretching. With this consideration and after some manipulation, the normalized thin-film equation reads as

$$\underbrace{\frac{\partial}{\partial \eta}\left(F^3 \frac{\partial^3 F}{\partial \eta^3}\right)}_{\Lambda_1} = \underbrace{3\mathrm{Ca}\left(\frac{\ell_x}{\ell_h}\right)^3 \frac{\partial F}{\partial \eta}}_{\Lambda_2} + \underbrace{\frac{R_m^2 \ell_x^2}{\ell_h^4} \frac{\partial}{\partial \eta}\left(\frac{1}{F}\frac{\partial F}{\partial \eta}\right)}_{\Lambda_3}. \tag{12}$$

In long bubble dynamics, we must have

$$O(\Lambda_1) = O(\Lambda_2) \Rightarrow 3\mathrm{Ca}\left(\frac{\ell_x}{\ell_h}\right)^3 = 1 \Rightarrow \frac{\ell_h}{\ell_x} = \mathscr{C}, \tag{13}$$

where $\mathscr{C} = (3\mathrm{Ca})^{1/3}$. Note that, following Bretherton's approach [1] by assuming $\ell_h = h_0$ and $\ell_x = h_0/\mathscr{C}$, criterion (13) is automatically satisfied, balancing surface tension effect with viscous effect. However, for disjoining pressure contribution to be effective, there must be a balance between the contributions of disjoining pressure with the other two effects. This essentially denotes

$$O(\Lambda_1) = O(\Lambda_3) \Rightarrow \frac{\ell_h^2}{\ell_x} = R_m. \tag{14}$$

Using Eqs. (13) and (14), we finally obtain the relevant characteristic length scales as

$$\ell_h = R_m/\mathscr{C} \quad \text{and} \quad \ell_x = R_m/\mathscr{C}^2. \tag{15}$$

Note that, from Eq. (15), the characteristic lengths are now dependent on both intrinsic molecular length scale (R_m) and capillary number (Ca). Thus, Eq. (15) represents the characteristic length scales governing the underlying physics, that are obtained from suitable combination of capillary number and the physics driven intrinsic length scales (the molecular length scale R_m for the present case).

With this argument, the normalized thin-film equation (12) reads as

$$\frac{\partial}{\partial \eta}\left(F^3 \frac{\partial^3 F}{\partial \eta^3}\right) = \frac{\partial F}{\partial \eta} + \frac{\partial}{\partial \eta}\left(\frac{1}{F}\frac{\partial F}{\partial \eta}\right). \tag{16}$$

Using Eq. (16) and invoking the definition $\mathscr{C} = (3\mathrm{Ca})^{1/3}$, the functional form of the thin-film profile (or the bubble profile), can now be given as

$$h(x; R_m, \mathrm{Ca}) = \frac{R_m}{(3\mathrm{Ca})^{1/3}} F\left[\frac{x}{R_m}(3\mathrm{Ca})^{2/3}\right]. \tag{17}$$

TABLE I. The characteristic length scales at different regimes, with consideration of van der Waals interaction in the disjoining pressure.

	ℓ_h	ℓ_x
Two-thirds power law regime	h_0	$h_0/(3\mathrm{Ca})^{1/\beta}$
van der Waals interaction regime	$R_m/(3\mathrm{Ca})^{1/\beta}$	$R_m/(3\mathrm{Ca})^{2/\beta}$

Equation (16) aptly retains the contribution of van der Waals interaction with consistent order of magnitude. Now we solve Eq. (16) numerically, following the same approach as employed for Eq. (4), with the criteria (5) and (6). The dotted line in Fig. 2 is from the solution of Eq. (16). The matching of this solution with the solution of the original thin-film equation (4) and Chen's [2] experimental observations is suggestive of the accuracy of the present scaling analysis to bring out the essential physics of interest. Since the scaling analysis is valid for the van der Waals interaction regime, the estimation from Eq. (16) departs from the estimation from both the original thin-film equation (4) and Chen's [2] experimental observations, as the two-thirds power law regime is approached.

With the aforementioned arguments and comparisons in the background, therefore, we can postulate that taking the van der Waals interaction into account in the disjoining pressure, the long bubble dynamics is governed by different characteristic length scales, as indicated in the Table I, for the sake of comprehensiveness. In a somewhat higher capillary number limit, the Bretherton scaling analysis seems to be valid. This eventually makes the disjoining pressure contribution negligible. Thus, to the leading order approximation, one can recover the exact Bretherton-Landau-Levich formalism, leading towards the two-thirds power law based estimation. In the very low capillary number regime, on the other hand, the bubble dynamics is governed by completely different length scales, as obtained from a suitable combination of the intrinsic molecular length scale and the capillary number, as shown in Table I. With this accounting, one can properly uncover the thin film, and hence the long bubble, dynamics in the van der Waals interaction regime.

C. Benchmarking with dynamic contact angle problem

It is important to mention that the present thin-film based formalism is very similar to that of the thin-film based analysis of dynamic contact angle, often elucidated as the Landau-Levich type formalism of dynamic contact angle problems [28,29,31]. It is, therefore, enticing to benchmark the present estimation of the characteristic length scales, for unveiling the essential features of a dynamic contact angle related problem, taking van der Waals interaction into account. A schematic of a dynamic contact angle related problem is shown in Fig. 4, which we endeavor to use in benchmarking our idea.

Starting from Eq. (16), we integrate it once with respect to η and set the integration constant to zero, so as to obtain the modified version of the thin-film equation as

$$\frac{\partial^3 F_0}{\partial \eta^3} = \frac{1}{F_0^2} + \frac{1}{F_0^4}\frac{\partial F_0}{\partial \eta}. \tag{18}$$

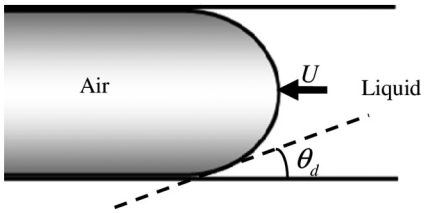

FIG. 4. Schematic of a liquid front moving with speed U while making a dynamic contact angle θ_d with the channel surface.

Equation (18) is exactly the same as that of the Landau-Levich type formalism for dynamic contact angle. Following the lead of Eggers and Stone [29], Eq. (18) can have the solution of the form

$$F_0 = A\eta\,[\ln(B\eta)]^{1/3}, \tag{19}$$

to the leading order approximation, in the limit $\eta \to \infty$, where one can define the contact angle. In Eq. (19), A and B are the constants of integration (for detailed derivations see Ref. [29]). Approximating dynamic contact angle $\theta_d = dh/dx$ in the small angle limit, and using Eq. (19) and the present scaling estimation (15), the dynamic contact angle relation can be recovered as

$$\theta_d^3 = 3A\mathrm{Ca}\ln\left(\frac{x}{L_c}\right), \tag{20}$$

to the leading order approximation, with

$$L_c = \frac{R_m}{B}(3\mathrm{Ca})^{-2/3} \tag{21}$$

as the characteristic length scale. Equation (21) represents the celebrated Tanner law for dynamic contact angle. Eggers and Stone [29] have shown that upon employing a suitable thin-film based formalism for dynamic contact angle problems, one may end up with a "model specific" characteristic length scale of the generic form Ca^{α} (with α being a real number). With consideration of the Lifshitz form of disjoining pressure, the generic form assumes the specific form, as shown in Eq. (21), and is similar to that shown in their study [29]. Such characteristic length scales are perfectly in tune with the experimental findings [30], even in the very low capillary number limit. Following this argument, we can say that our present scaling is acceptable to the limit that it can bring out the essential physics of interest.

IV. EFFECT NONUNIFORMITY IN BUBBLE PROFILE

So far we have considered the classical Lifshitz form of disjoining pressure, as given in Eq. (3). However, in reality, the disjoining pressure varies with the local slope and curvature of the thin-film profile [18,19,24]. With this accounting, the disjoining pressure can be given as [19]

$$\Pi = -\frac{A_H}{6\pi h^3}\Xi, \tag{22}$$

where

$$\Xi = 1 - \frac{3}{4}\left\{\left(\frac{\partial h}{\partial x}\right)^2 - h\frac{\partial^2 h}{\partial x^2}\right\} \tag{23}$$

acts as the correction due to nonuniformity in film thickness (see Appendix for details). With this argument, the thin-film equation assumes the form

$$\frac{\partial}{\partial x}\left(h^3\frac{\partial^3 h}{\partial x^3}\right) = 3\mathrm{Ca}\frac{\partial h}{\partial x} + R_m^2\frac{\partial}{\partial x}\left(\frac{\Xi}{h}\frac{\partial h}{\partial x} - \frac{1}{3}\frac{\partial \Xi}{\partial x}\right). \tag{24}$$

Now, we follow the similar stretching transformation strategy $h = \ell_h F$ and $x = \ell_x \eta$ [Eq. (15)], and obtain the normalized thin-film equation of the form

$$\underbrace{\frac{\partial}{\partial \eta}\left(F^3\frac{\partial^3 F}{\partial \eta^3}\right)}_{\Lambda_1} = \underbrace{3\mathrm{Ca}\left(\frac{\ell_x}{\ell_h}\right)^3\frac{\partial F}{\partial \eta}}_{\Lambda_2} + \underbrace{\frac{R_m^2\ell_x^2}{\ell_h^4}\frac{\partial}{\partial \eta}\left(\frac{\Xi}{F}\frac{\partial F}{\partial \eta} - \frac{1}{3}\frac{\partial \Xi}{\partial \eta}\right)}_{\Lambda_3}, \tag{25}$$

where the correction term reads as

$$\Xi = 1 - \left(\frac{\ell_h}{\ell_x}\right)^2\frac{3}{4}\left[\left(\frac{\partial F}{\partial \eta}\right)^2 - F\frac{\partial^2 F}{\partial \eta^2}\right]. \tag{26}$$

Employing the consistent order of magnitude considerations, we obtain the intrinsic length scales as

$$\begin{aligned} O(\Lambda_1) = O(\Lambda_2) \quad &\text{and} \quad O(\Lambda_1) = O(\Lambda_3) \\ \Rightarrow \ell_h = R_m/\mathscr{C} \quad &\text{and} \quad \ell_x = R_m/\mathscr{C}^2. \end{aligned} \tag{27}$$

Thus, the characteristic length scales remains the same as in Eq. (15). This transforms the thin-film equation into the form

$$\frac{\partial}{\partial \eta}\left(F^3\frac{\partial^3 F}{\partial \eta^3}\right) = \frac{\partial F}{\partial \eta} + \frac{\partial}{\partial \eta}\left(\frac{\Xi}{F}\frac{\partial F}{\partial \eta} - \frac{1}{3}\frac{\partial \Xi}{\partial \eta}\right), \tag{28}$$

where the correction term assumes the form

$$\Xi = 1 - \mathscr{C}^2\underbrace{\frac{3}{4}\left[\left(\frac{\partial F}{\partial \eta}\right)^2 - F\frac{\partial^2 F}{\partial \eta^2}\right]}_{\Psi}. \tag{29}$$

In contrast to the normalized thin-film equation (16), Eqs. (28) and (29) demonstrate the contribution of the correction term in disjoining pressure due to nonuniformity in film thickness.

The accommodation of the correction in disjoining pressure due to nonuniformity in the film thickness seems to be rational, owing to the typical bubble profile. However, our previous arguments and comparisons show that even without incurring such correction, it is sufficient to demonstrate the essential physics of interest. For the sake of further verification, we solve the thin-film equations (16) and (28). The bubble profiles, so obtained, are plotted in Fig. 5. The figure aptly reveals that the contribution of the correction in disjoining pressure, due to nonuniformity in film thickness, can be neglected, without any loss of generality. This is, nevertheless, quite contrary to the common expectation.

It is important to mention that the characteristic length scales remain the same for both the cases with and without slope and curvature dependence of disjoining pressure [compare Eqs. (15) and (27)]. Following Eqs. (28) and (29) and invoking the definition $\mathscr{C} = (3\mathrm{Ca})^{1/3}$, the functional form

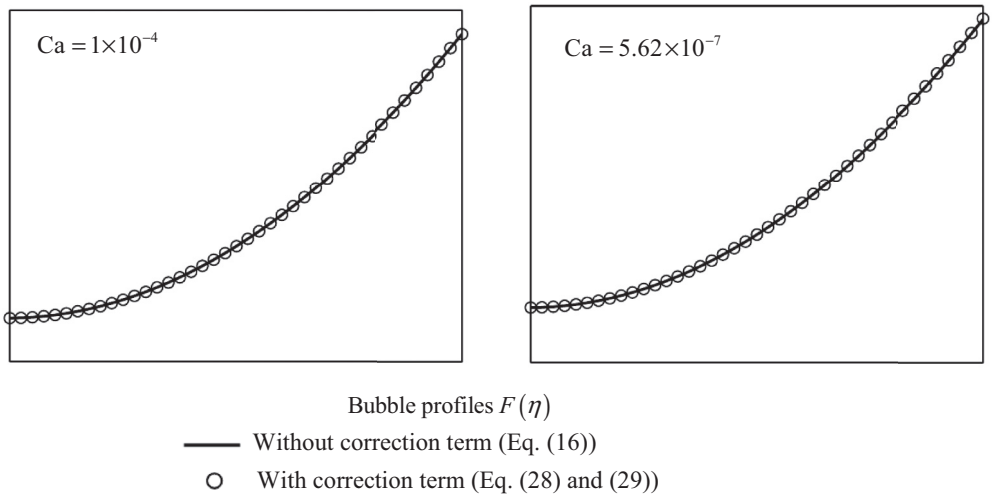

FIG. 5. Comparison of the bubble profiles $F(\eta)$ without and with accommodation of the correction due to slope and curvature dependence of disjoining pressure.

of the thin-film profile (or the bubble profile), can now be given as

$$h(x;R_m,\mathrm{Ca}) = \frac{R_m}{(3\mathrm{Ca})^{1/3}} F\left[\frac{x}{R_m}(3\mathrm{Ca})^{2/3};(3\mathrm{Ca})^{2/3}\right]. \quad (30)$$

In comparison to Eq. (17), the $(3\mathrm{Ca})^{2/3}$ contribution emerges out of the correction in disjoining pressure. Now, we can represent Eq. (30) as $h(3\mathrm{Ca})^{1/3}/R_m = F(\eta;\xi)$, where $\eta = x(3\mathrm{Ca})^{2/3}/R_m$ and $\xi = (3\mathrm{Ca})^{2/3}$. In the low Ca limit, we can expand $F(\eta;\xi)$ as

$$F(\eta;\xi) = F_0(\eta) + \xi F_1(\eta) + O(\xi^2). \quad (31)$$

Now, for the sake of comprehensiveness, we rewrite Eq. (28) as

$$\frac{\partial}{\partial\eta}\left(F^3\frac{\partial^3 F}{\partial\eta^3}\right) = \frac{\partial F}{\partial\eta} + \frac{\partial}{\partial\eta}\left(\frac{1}{F}\frac{\partial F}{\partial\eta}\right) - \xi\Omega, \quad (32)$$

where

$$\Omega = \frac{\partial}{\partial\eta}\left(\frac{\Psi}{F}\frac{\partial F}{\partial\eta}\right) - \frac{1}{3}\frac{\partial^2\Psi}{\partial\eta^2}, \quad (33)$$

with Ψ being defined as indicated in Eq. (29). Therefore, Ω carries the effect of slope and curvature dependence of disjoining pressure. To bring out the contribution of the term $\xi\Omega$ in Eq. (32), we first note that the term Ψ is reducible to the form

$$\begin{aligned}\Psi &= \underbrace{\frac{3}{4}\left[\left(\frac{\partial F_0}{\partial\eta}\right)^2 - F_0\frac{\partial^2 F_0}{\partial\eta^2}\right]}_{\Psi_0} \\ &\quad + \xi\underbrace{\frac{3}{4}\left[2\frac{\partial F_0}{\partial\eta}\frac{\partial F_1}{\partial\eta} - F_0\frac{\partial^2 F_1}{\partial\eta^2} - F_1\frac{\partial^2 F_0}{\partial\eta^2}\right]}_{\Psi_1} + O(\xi^2) \\ &= \Psi_0 + \xi\Psi_1 + O(\xi^2). \end{aligned} \quad (34)$$

Now, using Eqs. (31), (33), and (34), we can approximate Ω as

$$\Omega = \Omega_0 + \xi\Omega_1 + O(\xi^2)$$

with

$$\Omega_0 = \frac{\partial}{\partial\eta}\left(\frac{\Psi_0}{F_0}\frac{\partial F_0}{\partial\eta}\right) - \frac{1}{3}\frac{\partial^2\Psi_0}{\partial\eta^2} \quad \text{and}$$

$$\Omega_1 = \frac{\partial}{\partial\eta}\left[\frac{1}{F_0}\left(\Psi_0\frac{\partial F_1}{\partial\eta} + \Psi_1\frac{\partial F_0}{\partial\eta} - \Psi_0\frac{F_1}{F_0}\frac{\partial F_0}{\partial\eta}\right)\right] - \frac{1}{3}\frac{\partial^2\Psi_1}{\partial\eta^2}. \quad (35)$$

Therefore, the contribution of the term $\xi\Omega$ in Eq. (32) is reducible to the form

$$\varepsilon\Omega = \varepsilon\Omega_0 + \varepsilon^2\Omega_1 + O(\varepsilon^3). \quad (36)$$

Following Eqs. (31)–(36), therefore, Eq. (32) can be represented, to the different orders of magnitude, as

$$\begin{aligned} O(\xi^0):&\ \frac{\partial}{\partial\eta}\left(F_0^3\frac{\partial^3 F_0}{\partial\eta^3}\right) = \frac{\partial F_0}{\partial\eta} + \frac{\partial}{\partial\eta}\left(\frac{1}{F_0}\frac{\partial F_0}{\partial\eta}\right), \text{ and} \\ O(\xi^1):&\ \frac{\partial}{\partial\eta}\left(F_0^3\frac{\partial^3 F_1}{\partial\eta^3} + 3F_0^2F_1\frac{\partial^3 F_0}{\partial\eta^3}\right) \\ &= \frac{\partial F_1}{\partial\eta} + \frac{\partial}{\partial\eta}\left[\frac{1}{F_0}\left(\frac{\partial F_1}{\partial\eta} - \frac{F_1}{F_0}\frac{\partial F_0}{\partial\eta}\right)\right] \\ &\quad - \frac{\partial}{\partial\eta}\left(\frac{\Psi_0}{F_0}\frac{\partial F_0}{\partial\eta}\right) + \frac{1}{3}\frac{\partial^2\Psi_0}{\partial\eta^2}. \end{aligned} \quad (37)$$

From Eq. (37) it is evident that the leading order approximation recovers the thin-film equation (16). The higher order approximations contain the contribution of slope and curvature dependence of disjoining pressure, through accounting of Ω. Moreover, following Eq. (37), to the leading order approximation, the thin-film profile can be represented as

$$h = \frac{R_m}{(3\mathrm{Ca})^{1/3}} F_0\left[\frac{x}{R_m}(3\mathrm{Ca})^{2/3}\right], \quad (38)$$

recovering the same notion as in Eq. (17). Therefore, we can state that to the leading order approximation, it is sufficient to impose the Lifshitz form of disjoining pressure $-A_H/6\pi h^3$, for unveiling essential physics of long bubble dynamics, under the influence of van der Waals interaction. At the same time, abiding by the present scaling estimation, it is possible to bring out the order of magnitude contribution of the slope and curvature dependence of disjoining pressure which is following a two-thirds power relationship with capillary number [see Eq. (30)].

V. INFLUENCE OF THE ELECTROSTATIC COMPONENT OF DISJOINING PRESSURE

The electrostatic component of disjoining pressure becomes important when the carrier liquid is an electrolyte solution [13,20,23,27]. Charges from the electrolyte solution accumulate over the channel surface. If there are any surface active agents, such as surfactants, the charges also accumulate over the bubble interface. The situation, in absence of any external electric field, pertains to the following set of governing transport equations and boundary conditions [13]:

$$\left.\begin{aligned} &\text{Momentum:} \quad \frac{\partial p}{\partial x} = \mu \frac{\partial^2 u}{\partial y^2}, \ \text{with} \ u(0) = -U \ \text{and} \ u(h) = 0 \\ &\text{Continuity:} \quad \frac{\partial}{\partial x}\int_0^h u\,dy = 0 \end{aligned}\right\}. \tag{39}$$

The traction generated over the bubble interface, due to the adsorption of the surface active agents, allows the imposition of the no-slip boundary condition without any loss of generality [13]. The normal stress balance (2) reads as [13,20,23,27]

$$p = p_0 - \sigma \frac{\partial^2 h}{\partial x^2} \overbrace{\underbrace{-\frac{A_H}{6\pi h^3}}_{\Pi} \underbrace{-\frac{\varepsilon\varepsilon_0}{2h^2}\left(\frac{\pi k_B T}{Ze}\right)^2}_{\Pi_{es}}}^{\Sigma}. \tag{40}$$

In addition to van der Waals contribution Π, the disjoining pressure now has an electrostatic component Π_{es} due to the surface charges. Here $\varepsilon_0 = 8.85 \times 10^{-12}$ F/m is the permittivity of the free space, $k_B = 1.38 \times 10^{-23}$ kg m^2/K s^2 is the Boltzmann constant, and $e = 1.6 \times 10^{-19}$ C is the elementary charge [13,20,23,27]. In Eq. (40) Z, T, and ε represents the charge dissociated ion, temperature (in absolute scale), and the dielectric constant of the carrier liquid medium. For the present study, we consider $\varepsilon = 78$ (aqueous solution), $Z = 1$, and $T = 300$ K (the normal room temperature condition) [13,20,23,27]. Upon solving Eq. (39), and using Eq. (40), one can get the thin-film equation of the form

$$\frac{\partial}{\partial x}\left(h^3 \frac{\partial^3 h}{\partial x^3}\right) = 6\mathrm{Ca}\frac{\partial h}{\partial x} + R_m^2 \frac{\partial}{\partial x}\left(\frac{1}{h}\frac{\partial h}{\partial x}\right) + L_{es}\frac{\partial^2 h}{\partial x^2}, \tag{41}$$

where $L_{es} = (\varepsilon\varepsilon_0/4\sigma)(\pi k_B T/Ze)^2$ represents the physics driven intrinsic length scale due to surface charge effect.

We now solve Eq. (41) iteratively following the approach, as discussed previously. The h_0/R variation, so obtained, is plotted against Ca, as shown in Fig. 6. For the sake of comparison, we also plot the solution from Eq. (4) and the two-thirds power law based estimations. Moreover, Chen's [2] experimental observations with air bubbles are also presented in the figure. Additionally, in the same figure, we also present the solution of the rescaled Eq. (51); its implications are delineated *a posteriori*. First of all, we note that the electrostatic component of disjoining pressure endorses a higher film thickness, in all the ranges of Ca considered here. In a somewhat higher capillary number regime, though the film thickness follows two-thirds power law behavior, it matches with the estimation $h_0/R = 1.02\,(3\mathrm{Ca})^{2/3}$, in contrast with the conventional estimation [1] $h_0/R = 0.643\,(3\mathrm{Ca})^{2/3}$. It is also important to note that Chen's [2] experimental observation with air bubbles, as presented in Fig. 6, seems to match the estimation $h_0/R = 1.02\,(3\mathrm{Ca})^{2/3}$ in the higher capillary number regime. Such behavior can be attributed to the traction generated over the bubble interface, which makes it behave like an immobile surface [1,2,9,11]. In reality, maintaining absolute cleanliness during experiment is difficult. The presence of impurities, even in trace amounts, may alter the air-bubble dynamics. This feature is often argued to be responsible for mismatching of the estimation $h_0/R = 0.643\,(3\mathrm{Ca})^{2/3}$ while experimenting with air bubbles [1,2,9,11]. This is indicative of the fact that the bubble dynamics in the presence of surface charge is primarily dictated by the traction generated on the bubble interface, in the two-thirds power law regime. In the very low capillary number regime, the electrostatic component seems to play a significant role. Thus, we obtain somewhat higher film thickness than that obtained from considering the van der Waals interaction only. Therefore, we earmark this deviant regime as the electrostatic interaction regime. It is now imperative to unveil the underlying physics leading to the aforementioned behaviors.

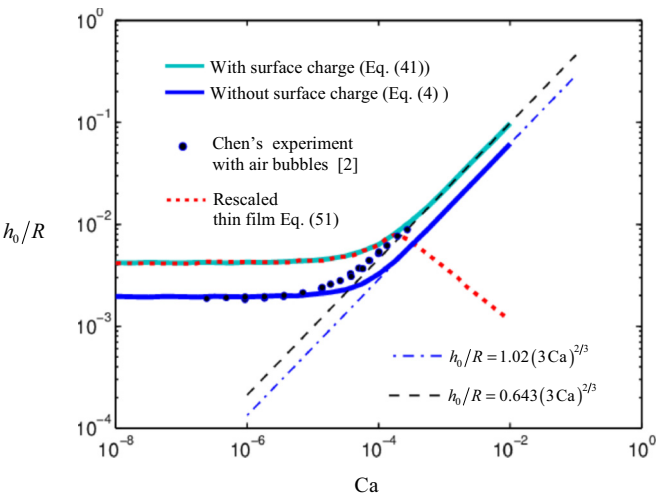

FIG. 6. (Color online) Comparison of the variation of h_0/R with Ca, with and without consideration of the surface charge effect.

A. The two-thirds power law regime

Starting from Eq. (41) we impose the similar stretching transformation strategy $h = \ell_h F$ and $x = \ell_x \eta$ [Eq. (15)], and obtain the normalized thin-film equation of the form

$$\underbrace{\frac{\partial}{\partial\eta}\left(F^3\frac{\partial^3 F}{\partial\eta^3}\right)}_{\Lambda_1} = \underbrace{6\mathrm{Ca}\left(\frac{\ell_x}{\ell_h}\right)^3\frac{\partial F}{\partial\eta}}_{\Lambda_2} + \underbrace{\frac{R_m^2\ell_x^2}{\ell_h^4}\frac{\partial}{\partial\eta}\left(\frac{1}{F}\frac{\partial F}{\partial\eta}\right)}_{\Lambda_3} + \underbrace{\frac{L_{es}\ell_x^2}{\ell_h^3}\frac{\partial^2 F}{\partial\eta^2}}_{\Lambda_4}. \quad (42)$$

The term Λ_4 emerges out of the electrostatic interaction. The existence of two-thirds power law type behavior is suggestive of the validity of the Bretherton scaling argument [1]. This argument, on the other hand, emanates, essentially, from the balance between the surface tension and the viscous effect. Imposing this argument, from Eq. (42), we obtain

$$O(\Lambda_1) = O(\Lambda_2) \Rightarrow 6\mathrm{Ca}\left(\frac{\ell_x}{\ell_h}\right)^3 = 1 \Rightarrow \frac{\ell_h}{\ell_x} = \mathscr{C}. \quad (43)$$

Note that here $\mathscr{C} = (6\mathrm{Ca})^{1/3}$, which is higher than the previous consideration of $\mathscr{C}$. Now we consider $\ell_h = h_0$, and following Eq. (43) we obtain $\ell_x = h_0/\mathscr{C}$. With this argument, Eq. (42) transforms to the form

$$\frac{\partial}{\partial\eta}\left(F^3\frac{\partial^3 F}{\partial\eta^3}\right) = \frac{\partial F}{\partial\eta} + \underbrace{\frac{R_m^2}{h_0^2(6\mathrm{Ca})^{2/3}}}_{\varepsilon_\Pi}\frac{\partial}{\partial\eta}\left(\frac{1}{F}\frac{\partial F}{\partial\eta}\right) + \underbrace{\frac{L_{es}}{h_0(6\mathrm{Ca})^{2/3}}}_{\varepsilon_{\Pi_{es}}}\frac{\partial^2 F}{\partial\eta^2}. \quad (44)$$

The factors ε_Π and $\varepsilon_{\Pi_{es}}$ denote the order of magnitude contribution of Π and Π_{es} respectively, in the two-thirds power law regime. In Fig. 7 we demonstrate the variation of the factors ε_Π and $\varepsilon_{\Pi_{es}}$ with Ca. Note that in the two-thirds power law regime, both ε_Π and $\varepsilon_{\Pi_{es}}$ are less than unity. In the electrostatic interaction regime, on the other hand, their magnitudes are well higher than unity, demonstrating the breakdown of the scaling estimations $\ell_h = h_0$ and $\ell_x = h_0/\mathscr{C}$, at the same time, indicating the existence of different characteristic length scales. Nevertheless, in all the regimes $\varepsilon_{\Pi_{es}} > \varepsilon_\Pi$. For the sake of further clarification, in the inset of Fig. 7, we also plot $\gamma = \varepsilon_\Pi/\varepsilon_{\Pi_{es}}$ against Ca. Evidently, $\gamma < 1$ in all the regimes, indicating the suppression of the contribution of Π under the presence of the contribution of Π_{es}. It is also noteworthy that in the two-thirds power law regime $\gamma \ll 1$.

For the sake of further analysis, we first rewrite Eq. (44) as

$$\frac{\partial}{\partial\eta}\left(F^3\frac{\partial^3 F}{\partial\eta^3}\right) = \frac{\partial F}{\partial\eta} + \gamma\varepsilon_{\Pi_{es}}\frac{\partial}{\partial\eta}\left(\frac{1}{F}\frac{\partial F}{\partial\eta}\right) + \varepsilon_{\Pi_{es}}\frac{\partial^2 F}{\partial\eta^2}. \quad (45)$$

Thus, the film profile function can be represented as $h/h_0 = F(\eta;\gamma,\varepsilon_{\Pi_{es}})$, allowing an expansion of the form

$$F\left(\eta;\gamma,\varepsilon_{\Pi_{es}}\right) = F_0(\eta;\gamma) + \varepsilon_{\Pi_{es}}F_1(\eta;\gamma) + O\left(\varepsilon_{\Pi_{es}}^2\right). \quad (46)$$

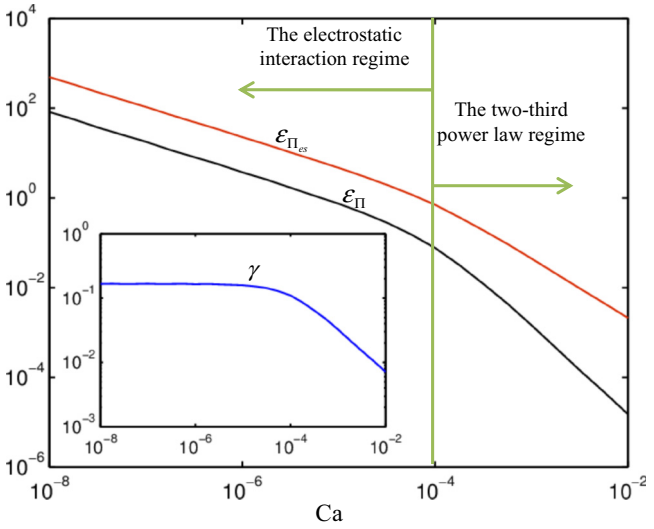

FIG. 7. (Color online) Variation of ε_Π and $\varepsilon_{\Pi_{es}}$ with Ca. The inset shows the variation of $\gamma = \varepsilon_\Pi/\varepsilon_{\Pi_{es}}$ with Ca. Similar to Fig. 3, the demarcation between the two regimes is to be considered as the representative demonstration of the essential features.

Using Eq. (46), the scaled film equation (45) reduces to the form, at different orders, as

$$O\left(\varepsilon_{\Pi_{es}}^0\right): \frac{\partial}{\partial\eta}\left(F_0^3\frac{\partial^3 F_0}{\partial\eta^3}\right) = \frac{\partial F_0}{\partial\eta},$$

$$O\left(\varepsilon_{\Pi_{es}}^1\right): \frac{\partial}{\partial\eta}\left(F_0^3\frac{\partial^3 F_1}{\partial\eta^3} + 3F_0^2F_1\frac{\partial^3 F_0}{\partial\eta^3}\right) = \frac{\partial F_1}{\partial\eta} + \gamma\frac{\partial}{\partial\eta}\left(\frac{1}{F_0}\frac{\partial F_0}{\partial\eta}\right) + \frac{\partial^2 F_0}{\partial\eta^2}. \quad (47)$$

Thus, from Eq. (47) we can see that the leading order of approximation recovers the Bretherton-Landau-Levich type formalism, albeit with slightly different scaling. Moreover, the contribution of Π and Π_{es} gets transferred to the higher order approximations. This is in tune with the fact that the bubble dynamics is primarily decided by the traction generated over the bubble interface, as anticipated previously. Likewise, upon solving the leading order equation, we obtain $\partial^2 F_0/\partial\eta^2 = 0.643$, as $\eta \to \infty$. This eventually provides $h_0/R = (\lim_{\eta\to\infty}\partial^2 F_0/\partial\eta^2)(6\mathrm{Ca})^{2/3} = 1.012\,(3\mathrm{Ca})^{2/3}$, as predicted previously.

B. The electrostatic interaction regime

In the electrostatic interaction regime, the scaling arguments $\ell_h = h_0$ and $\ell_x = h_0/\mathscr{C}$ break down, as shown previously. Thus, by beginning with the general notion, $x = \ell_x\eta$ and $h = \ell_h F$, we finally end up with the scaled thin-film equation (42). Here, the primary criterion (43) also holds true. Additionally, for any perceptible contribution of the electrostatic component of the disjoining pressure, we must have

$$O(\Lambda_1) = O(\Lambda_4) \Rightarrow \frac{L_{es}\ell_x^2}{\ell_h^3} = 1 \Rightarrow \frac{\ell_h^3}{\ell_x^2} = L_{es}. \quad (48)$$

Using Eqs. (43) and (48), therefore, we obtain the consistent length scales as

$$\ell_h = L_{es}/\mathscr{C}^2 \quad \text{and} \quad \ell_x = L_{es}/\mathscr{C}^3. \tag{49}$$

Now using Eq. (49) we can also estimate

$$O(\Lambda_3) = \frac{R_m^2 \ell_x^2}{\ell_h^4} = \underbrace{\frac{R_m^2 \mathscr{C}^2}{L_{es}^2}}_{\delta}. \tag{50}$$

Following the above-mentioned arguments, therefore, the normalized thin-film equation reads as

$$\frac{\partial}{\partial \eta}\left(F^3 \frac{\partial^3 F}{\partial \eta^3}\right) = \frac{\partial F}{\partial \eta} + \frac{\partial^2 F}{\partial \eta^2} + \delta \frac{\partial}{\partial \eta}\left(\frac{1}{F}\frac{\partial F}{\partial \eta}\right). \tag{51}$$

Thus, the functional form of the film profile function can be given as

$$h(x; L_{es}, \mathrm{Ca}, R_m) = \frac{L_{es}}{(6\mathrm{Ca})^{2/3}} F\left[\frac{x}{L_{es}}(6\mathrm{Ca}); \frac{R_m^2}{L_{es}^2}(6\mathrm{Ca})^{2/3}\right]. \tag{52}$$

In contrast to the predominance of traction driven bubble dynamics in the two-thirds power law regime, Eq. (51) aptly retains the consistent order of magnitude contribution of the electrostatic component of disjoining pressure, following the consistent scaling arguments (49). The factor $R_m^2 (6\mathrm{Ca})^{2/3}/L_{es}^2$ in Eq. (52) emanates from the contribution of the van der Waals component of disjoining pressure. Now we solve Eq. (51) iteratively and obtain the variation of minimum film thickness with capillary number. The dotted line in Fig. 6 demonstrates this variation. Within the zone of validation of the scaling estimation (49), and the subsequent thin-film equation (51), we find a very satisfactory matching with the original thin-film equation (41), as shown in Fig. 6. This essentially demonstrates the validity of the present scaling estimation to capture the essential physics of interest, in the electrostatic interaction regime.

Finally we note that the van der Waals component of disjoining pressure endorses an $O(\delta) = O[R_m^2 (6\mathrm{Ca})^{2/3}/L_{es}^2]$ contribution in the bubble dynamics. Taking consistent data from the literature, one can easily find that $\delta \ll 1$, in the electrostatic interaction regime. Thus, we can expand $F(\eta; \delta)$ as

$$F(\eta; \delta) = F_0(\eta) + \delta F_1(\eta) + O(\delta^2). \tag{53}$$

Imposing the expansion (53), Eq. (51) is now reducible to

$$\begin{aligned} O(\delta^0): &\ \frac{\partial}{\partial \eta}\left(F_0^3 \frac{\partial^3 F_0}{\partial \eta^3}\right) = \frac{\partial F_0}{\partial \eta} + \frac{\partial^2 F_0}{\partial \eta^2}, \\ O(\delta^1): &\ \frac{\partial}{\partial \eta}\left(F_0^3 \frac{\partial^3 F_1}{\partial \eta^3} + 3F_0^2 F_1 \frac{\partial^3 F_0}{\partial \eta^3}\right) \\ &= \frac{\partial F_1}{\partial \eta} + \frac{\partial^2 F_1}{\partial \eta^2} + \frac{\partial}{\partial \eta}\left(\frac{1}{F_0}\frac{\partial F_0}{\partial \eta}\right). \end{aligned} \tag{54}$$

Note that the leading order approximation does not contain any contribution of Π; it is realized in the higher order approximations. For the sake of verification we compare the variation of minimum film thickness as obtained from solving Eq. (51) with that of its leading order approximation, Eq. (54),

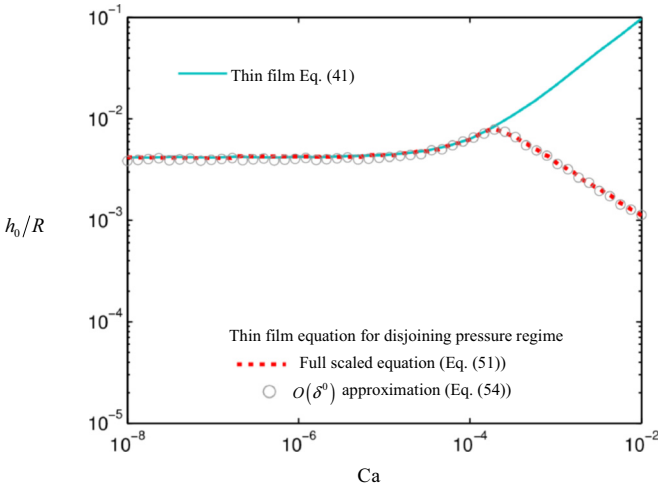

FIG. 8. (Color online) Comparison of the h_0/R variation with Ca, as obtained from the full scaled Eq. (51) and its $O(\delta^0)$ approximation from Eq. (54). For the sake of comprehensiveness, in the figure, we also show the results from the original thin-film Eq. (41).

as shown in Fig. 8. From the close matching of the two solutions, it is now quantitative that under the presence of surface charges, the electrostatic component of disjoining pressure well surpasses the van der Waals interaction to dictate the long bubble dynamics, indicating the significance of considering the electrostatic component of disjoining pressure, in the presence of surface charges. Such behaviors are perfectly in tune with other reported observations [13,23,27].

Thus, we have seen that taking the electrostatic interaction into consideration, by introducing the corresponding electrostatic component of disjoining pressure, the long bubble dynamics is governed by different characteristic length scales, as indicated in Table II, for the sake of comprehensiveness. In a somewhat higher capillary number limit, the bubble dynamics is primarily governed by the traction generated over the bubble interface, leading towards a Bretherton-Landau-Levich type description of the bubble dynamics without incurring, to the leading order approximation, much contribution from the van der Waals interaction and the electrostatic component. In the low capillary number regime the contribution of the electrostatic component starts to play a significant role. Under this circumstance, the bubble dynamics is decided by the intrinsic length scale L_{es} and the capillary number; their suitable combinations, as shown in the Table II, provide the characteristic length scales governing the underlying physics.

TABLE II. The characteristic length scales at different regimes, with consideration of the electrostatic interaction in the disjoining pressure.

	ℓ_h	ℓ_x
Two-thirds power law regime	h_0	$h_0/(6\mathrm{Ca})^{1/3}$
Electrostatic interaction regime	$L_{es}/(6\mathrm{Ca})^{2/3}$	$L_{es}/(6\mathrm{Ca})$

VI. CONCLUSIONS

In conclusion, we theoretically study the influence of disjoining pressure for moving long bubbles inside cylindrical capillaries. Towards that end, consistent thin-film equations, for the annular region separating the bubble from the channel surface, are presented with specific emphasis, and a consistent accounting of three different attributes: (a) the van der Waals interaction, as formalized by classical Lifshitz form of disjoining pressure; (b) the nonuniformity in film thickness, as accommodated by the necessary corrections in the disjoining pressure; and (c) the electrostatic component of disjoining pressure, reminiscent of the electrostatic interactions in the presence of surface charges. Taking van der Waals interaction into account, the resulting thin-film equation captures, in perfect agreement with previous experimental observations, both the celebrated two-thirds power behavior of the minimum film thickness and its departure in the very low capillary number regime. Consecutively we conduct scaling analysis, by employing stretching transformation followed by order of magnitude and subsequent asymptotic analysis of the resulting thin-film equation, and quantitatively demonstrate the dynamics of these two regimes, as decided by different characteristic length scales. Moreover, the characteristic length scales are found to be exactly the same as those governing the dynamics of dynamic contact angles. Our analysis reveals that the additional correction due to the slope and curvature dependence of disjoining pressure does not alter the characteristic length scales; however, it endorses a contribution which is significant to the order of the two-thirds power of the capillary number. The subsequent asymptotic analysis reveals that this correction may be neglected to the leading order approximation. Finally, we consider the electrostatic component of the disjoining pressure which may be realized in the presence of surface charges. Here we also find out a two-thirds power law behavior, of minimum film thickness, and its departure in the very low capillary number regime. The dynamics in the two-thirds power law regime seems to be primarily governed by the traction generated over the bubble interface. The significance of the electrostatic interaction is realized over a very small capillary number regime, leading towards the departure from the two-thirds power law type behavior. Subsequently, our scaling analysis quantitatively rationalizes these behaviors.

ACKNOWLEDGMENT

The authors would like to acknowledge Indian Academy of Sciences, Bangalore, for providing a fellowship to P.V.A., for undertaking a part of the present work.

APPENDIX: ON ACCOUNTING DISJOINING PRESSURE FOR NONUNIFORM THIN FILMS

Following the considerations of Dai *et al.* [19] and Wu and Wong [24], the interfacial free energy of the present situation of bubble in liquid medium can be given as

$$E_{\rm int} = \int_{x_1}^{x_2} \left(\sigma\sqrt{1+h_x^2} + \sigma_{\rm LS} - \sigma_{\rm SG} + E + \Delta p h\right) dx, \tag{A1}$$

where E denotes the excess free energy per unit area of the solid-liquid interfacial zone and Δp accounts for the Lagrange multiplier for mass conservation (eventually having the features of pressure). In Eq. (A1), $\sigma_{\rm LS}$ and $\sigma_{\rm SG}$ defines the interfacial energy per unit width in between the "liquid-solid" and "solid-gas" interfacial regions, respectively. Note that in the accounting of excess interfacial free energy, we do not account for the contribution of excess interfacial free energy outside the solid-liquid region. Accounting of such attributes is important for the analysis of contact line dynamics, since the energetic contribution of the solid-vapor region, outside the contact line region, plays a significant role in the underlying phenomenology [19,24]. However, for gas bubble in liquid medium, the existence of such region can be discarded without any loss of generality, for the background liquid to be perfectly wetting the channel surface.

Now, the excess free energy E can be a function of film thickness h and its axial gradients ($h_x^{(n)} = \partial^n h/\partial x^n$, where n can be any real, positive integer greater than zero). The energy minimizing principle demands

$$\frac{\delta E_{\rm int}}{\delta h} = -\frac{\sigma\partial^2 h/\partial x^2}{\{1+(\partial h/\partial x)^2\}^{3/2}} + \Delta p + \frac{\partial E}{\partial h} + \sum_n (-1)^n \frac{d^n}{dx^n}\left(\frac{\partial E}{\partial h_x^{(n)}}\right) = 0, \tag{A2}$$

from which one can define the Lagrange multiplier, hence the disjoining pressure, as

$$\Delta p = \frac{\sigma\partial^2 h/\partial x^2}{\{1+(\partial h/\partial x)^2\}^{3/2}} - \frac{\partial E}{\partial h} - \sum_n (-1)^n \frac{d^n}{dx^n}\left(\frac{\partial E}{\partial h_x^{(n)}}\right). \tag{A3}$$

The first term on the right-hand side of Eq. (A3) represents the Young-Laplace pressure jump, and can be given as $\sigma\partial^2 h/\partial x^2$, in the low capillary number limit [1,3,6,8,13]. The remaining terms on the right-hand side of Eq. (A3) represent disjoining pressure,

$$\Pi = -\frac{\partial E}{\partial h} - \sum_n (-1)^n \frac{d^n}{dx^n}\left(\frac{\partial E}{\partial h_x^{(n)}}\right). \tag{A4}$$

The classical definition of disjoining pressure is the gradient of excess interfacial free energy per unit width of the surface (i.e., $-\partial E/\partial h$) [19,21,24,26]. Compared to this, the augmentation in the definition of disjoining pressure emerges out of the nonuniformity in film thickness [19,24]. Therefore, the disjoining pressure contains the effects of film thickness and its axial gradients.

Following Dai *et al.* [19], from considerations of molecular interaction, E can be given as

$$E = -A_H\left[\frac{1}{12\pi h^2} + \frac{\left(h_x^{(1)}\right)^2}{16\pi h^2}\right], \tag{A5}$$

in the limit $|\partial h/\partial x| \ll 1$. For steadily moving long bubbles inside cylindrical capillaries, in the low capillary number limit, the small slope criteria ($|\partial h/\partial x| \ll 1$) remain valid as well [1,3,6,8,13]. Note that the second term on the right-hand side of

Eq. (A5) denotes the energy contribution due to nonuniformity in film thickness.

Now, using Eq. (A5) in Eq. (A4), the disjoining pressure can be given as

$$\Pi = -\frac{A_H}{6\pi h^3}\Xi, \tag{A6}$$

with

$$\Xi = 1 - \frac{3}{4}\left\{\left(\frac{\partial h}{\partial x}\right)^2 - h\frac{\partial^2 h}{\partial x^2}\right\}. \tag{A7}$$

This is the form of disjoining pressure, adopted for the present study.

[1] F. P. Bretherton, J. Fluid Mech. **10**, 166 (1961).
[2] J. Chen, J. Colloid Interface Sci. **109**, 341 (1986).
[3] S. R. Hodges, O. E. Jensen, and J. M. Rallison, J. Fluid Mech. **501**, 279 (2004).
[4] G. Karimi, in *Proceedings of the Ninth Intersociety Conference on Thermal and Thermomechanical Phenomena in Electronic Systems 2004. ITHERM '04* (IEEE, New York, 2004), p. 52.
[5] M. T. Kreutzer, F. Kapteijn, J. A. Moulijn, C. R. Kleijn, and J. J. Heiszwolf, AIChE J. **51**, 2428 (2005).
[6] Y.-C. Li, Y.-C. Liao, T.-C. Wen, and H.-H. Wei, J. Fluid Mech. **741**, 200 (2014).
[7] K. Mukundakrishnan, P. Ayyaswamy, and D. Eckmann, Phys. Rev. E **78**, 036303 (2008).
[8] M. Muradoglu and H. A. Stone, J. Fluid Mech. **570**, 455 (2007).
[9] J. Ratulowski and H.-C. Chang, J. Fluid Mech. **210**, 303 (1990).
[10] E. Sassaroli and K. Hynynen, J. Acoust. Soc. Am. **115**, 3235 (2004).
[11] K. J. Stebe and D. Barthès-Biesel, J. Fluid Mech. **286**, 25 (1995).
[12] H. A. Stone, A. D. Stroock, and A. Ajdari, Annu. Rev. Fluid Mech. **36**, 381 (2004).
[13] P. Takhistov, A. Indeikina, and H.-C. Chang, Phys. Fluids **14**, 1 (2002).
[14] G. I. Taylor, J. Fluid Mech. **10**, 161 (1961).
[15] S.-Y. Teh, R. Lin, L.-H. Hung, and A. P. Lee, Lab Chip **8**, 198 (2008).
[16] H. Wong, C. J. Radke, and S. Morris, J. Fluid Mech. **292**, 71 (1995).
[17] L. G. Leal, *Advanced Transport Phenomena* (Cambridge University Press, Cambridge, 2007).
[18] L. Biswal, S. K. Som, and S. Chakraborty, Int. J. Heat Mass Transfer **57**, 402 (2013).
[19] B. Dai, L. G. Leal, and A. Redondo, Phys. Rev. E **78**, 061602 (2008).
[20] B. Derjaguin and N. Churaev, J. Colloid Interface Sci. **49**, 249 (1974).
[21] I. E. Dzyaloshinskii, E. M. Lifshitz, and L. P. Pitaevskii, Sov. Phys. Usp. **4**, 153 (1961).
[22] A. Oron and S. G. Bankoff, Rev. Mod. Phys. **69**, 931 (1997).
[23] S. Pati, S. K. Som, and S. Chakraborty, Int. J. Heat Mass Transfer **64**, 304 (2013).
[24] Q. Wu and H. Wong, J. Fluid Mech. **506**, 157 (2004).
[25] H. Qiu and X. Wang, in *Proceedings of the 13th International Symposium on Applications of Laser Techniques to Fluid Mechanics, Lisbon*, Protugal, 2006, p. 26, http://ltces.dem.ist.utl.pt/lxlaser/lxlaser2006/.
[26] E. M. Lifshitz, Sov. Phys. JETP **2**, 73 (1956).
[27] S. Narayanan, A. G. Fedorov, and Y. K. Joshi, Langmuir **27**, 10666 (2011).
[28] S. Kalliadasis and H.-C. Chang, Phys. Fluids **6**, 12 (1994).
[29] J. Eggers and H. A. Stone, J. Fluid Mech. **505**, 309 (2004).
[30] J. A. Marsh, S. Garoff, and E. B. Dussan V., Phys. Rev. Lett. **70**, 2778 (1993).
[31] J. H. Snoeijer and B. Andreotti, Annu. Rev. Fluid Mech. **45**, 269 (2013).